Geometric modelling of the volume of investigation of well logs for thin-bed characterization

Masoudi Pedram, Hossein Memarian, Tahar Aifa, Behzad Tokhmechi

IOP Publishing Journal of Geophysics and Engineering
J. Geophys. Eng. 14 (2017) 426–444 (19pp) https://doi.org/10.1088/1742-2140/aa59d4

Geometric modelling of the volume of investigation of well logs for thin-bed characterization

Pedram Masoudi[1,2], Hossein Memarian[2,4], Tahar Aïfa[1,4] and Behzad Tokhmechi[3]

[1] Geosciences-Rennes, CNRS UMR6118, Université de Rennes 1, Bat 15, Campus de Beaulieu, F-35042 Rennes cedex, France
[2] School of Mining Engineering, College of Engineering, University of Tehran, North Kargar, 1431954378 Tehran, Iran
[3] Department of Petroleum Engineering, University of North Dakota, 243 Centennial Drive Stop 8154, Grand Forks, ND 58202-8154, USA

E-mail: memarian@ut.ac.ir and tahar.aifa@univ-rennes1.fr

Received 10 June 2016, revised 8 January 2017
Accepted for publication 17 January 2017
Published 10 March 2017

Abstract

The fuzzy membership function is used to model the volume of investigation of well logs geometrically. We discuss the fact that the spacing of a transmitter–receiver is not a precise parameter for addressing the vertical resolution of well logs. Instead, the vertical resolution of membership function (VRmf) is developed and estimated by variography analysis. In the five studied wells, the vertical resolution of gamma ray (GR), bulk density (RHOB), neutron porosity (NPHI) and sonic (DT) logs are estimated to be 61, 76, 76 and 61 cm, respectively. The simplest membership function for describing the volume of investigation of the GR, RHOB and NPHI is the triangle. For DT it is a complex shape. Being compatible with volumetric records in the well logs, the volumetric Nyquist frequency is introduced while considering the VRmf. Based on triangular membership functions, a thin-bed geometric simulator is designed. Regression models, i.e. deconvolution relations, are developed between the real thickness and the real petrophysical variation of a thin bed as outputs, and the same log-derived parameters are used as inputs. The shoulder-bed effect in GR, RHOB and NPHI is reduced by two to three times due to the mean squared error (MSE). To check the applicability of the deconvolution relations for the real data, ten thin beds are chosen within a well at the interval of the Sarvak Formation. In all the observations, the shoulder-bed effect is reduced after deconvolution. The thickness of the thin beds is estimated with a standard deviation of 4.4 cm, which is a precise value. The method is applied to the cored interval of the Sarvak Formation in a nearby well to characterize a porous carbonate thin bed sandwiched between dense carbonates. The estimated thin-bed thickness (13 $\pm$ 7.5 cm) is close to the *in situ* thin-bed thickness (<25 cm). Furthermore, the NPHI (total porosity) of the thin bed is estimated to be 11.7%, which is compatible with the core porosity (effective porosity), which is 8%, since the effective porosity should be less than the total porosity.

Keywords: volumetric Nyquist frequency, well log deconvolution, shoulder-bed effect, thin-bed simulator, thin-bed characterization

(Some figures may appear in colour only in the online journal)

[4] Authors to whom any correspondence should be addressed.

Abbreviations

API	American Petroleum Institute
ave	average
DT	sonic
$fr_{Nq,vol}$	volumetric Nyquist frequency
GR	gamma ray
mfT	membership function of transmitter
mfR	membership function of receiver
MSE	mean squared error
NPHI	neutron porosity
phi	porosity
reg	regression
RHOB	bulk density
slog	synthetic-log
SR	sampling rate
TH	thickness
VRmf	vertical resolution of membership function
VRT	vertical resolution of tool

1. Introduction

It has already been predicted that 'future exploration targets are likely to be thinner' for petroleum discoveries (Sengupta 1987 and Sengupta *et al* 1989). On the other hand, near-wellbore thin beds could be pinched out of larger sandy lenses, or related to other stratigraphic traps (Qi and Carr 2006). Thin beds could thus be stable productive horizons and developing thin-bed characterization methods is necessary for the future of the oil industry.

Well logs are continuous sensor recordings through wells that provide high-resolution petrophysical information to characterize geological layers. Despite their vast applications in sub-surface geology, there are some limitations regarding data acquisition for thin-bed studies. (i) The shoulder-bed effect, which refers to the effect of adjacent beds on well-logging measurements, especially when a thin bed is sandwiched between two thick beds. This effect is related to deconvolution of the real petrophysical profile, because of the vertical resolution of the measuring tool (RP 2007, Sanchez Ramirez *et al* 2010 and Torres-Verdín *et al* 2009). When the thickness of a layer falls below the vertical resolution of the tool, log-derived records and successive interpretations will become unreliable, e.g. the error of estimation for water saturation will be multiplied at least fourfold, and so will be overestimated (Bilardo *et al* 1996). It is also reported that shoulder- and bed-thickness effects can account for up to 33% and 31% of the *P*- and *S*-velocities, respectively, while the log responses are much less sensitive to laminations. In simulations, the results for sand-shale laminations only show variations of 16.4% and 3.6% in the *P*- and *S*-velocities, respectively (Peyret *et al* 2006). (ii) Sampling rate, which is mostly about 15.24 cm in the petroleum industry. Due to the well-known Nyquist frequency rule, there is no guarantee for characterizing geological strata thinner than 15.24 cm using well logs (Kinsland *et al* 2010).

Using finite element-based modelling within a thin-bedded turbiditic reservoir, researchers reduced the scale of the study from the well scale to the intermediate scale, i.e. the scale between cores and well-logs. Consequently, the geological uncertainties in estimating the vertical and horizontal permeability were reduced (Dubost *et al* 2004). In another work, within thin-layered limestone (St Louis, USA), an artificial neural network was trained by about ten cored wells to classify six major lithofacies using well logs: GR, resistivity (deep and medium), density (RHOB), neutron porosity (NPHI) and photoelectric (Dunham 1962). The prediction accuracy reached values between 70.37% and 90.82% (Qi and Carr 2006).

Two approaches are planned for porosity and water saturation estimation in thin-bed clastic formations (Torres-Verdín *et al* 2009). (i) The first approach is for beds that are thicker than 1 foot, and the inflection points of a vertical high-resolution log are defined as bed boundaries. (ii) The second approach is suitable for beds that are thinner than 1 foot, and is based on a novel Bayesian statistical inversion methodology (Tarantola 2005). The Bayesian inversion method overestimates hydrocarbon reserves by 26%, while the conventional methodology underestimates the reserve by 48% (Torres-Verdín *et al* 2009).

The underestimation of the hydrocarbon reserve by conventional interpretations has also been confirmed using an inverse methodology (Sanchez Ramirez *et al* 2010). This resulted in a 28% increase of the hydrocarbon reserve compared to conventional log interpretations. In addition, the inverse methodology provided 19% better agreement with core measurements. In similar works, it was stated that using inversion-based methods improves hydrocarbon pore volume and porosity estimation by 10% and 15%, respectively (Ijasan *et al* 2013, 2014). Another work concerning the effect of shoulder-beds revealed 50% overestimation of water saturation in conventional interpretations compared to the inversion-based method. The overestimation reaches 100% when there is a coincidence of invasion, shoulder-bed and well deviation (Ortega *et al* 2015).

In another paper, two inversion-based methodologies are devised for thin-bed characterization by RHOB, NPHI, photoelectric factor, GR/GR-spectroscopy and electrical resistivity logs. In the first methodology, the invasion effect (infiltration of drilling mud into the reservoir) is considered. The algorithm addresses quality control, necessary environmental corrections, an initial guess for the layer-by-layer petrophysical properties and non-linear inversion by minimizing the quadratic cost function. The outputs of the inversion are the volumetric concentrations of shale porosity, clay and silt. In the second methodology, the effect of mud filtrate is neglected. The identification error is revealed by synthetic datasets. In thin-bed (thickness of less than 61 cm) gas-bearing conditions, an error of at least 30% is reported. The error for estimating porosity, water saturation and shale volume is lower than 20%, but the error increases to 50% when estimating dolomite and calcite. It is interpreted that the

Table 1. Log characteristics of Sarvak Formation within the two wells, under study.

		GR (API)	RHOB (g cm^{-3})	NPHI (%)
Well #1	Average	8	2.52	14.7
	Standard deviation	7	1.09	6.5
Well #3	Average	8	2.54	10.4
	Standard deviation	6	1.24	6.7

shoulder-bed effect is the cause of the high errors (Heidari *et al* 2012).

The above methodology was later applied to characterize thin-bedded carbonate and organic-shale formations. It was found that for a thin bed a thickness of 15.2 cm with an uncertainty of 7.6 cm causes 35% and 48% errors in overestimating non-shale porosity and non-shale water saturation, respectively (Heidari and Torres-Verdín 2014).

An open-source Matlab package was developed to denoise well-log signals and provide the thickness, depth, mean, median and variance of each layer (Davis and Christensen 2013). It was also reported in the same paper that combining apparent conductivity and natural gamma logs provides a lithology scheme, distinguishing thicknesses up to about 50 cm.

In the literature, mathematical tools like numerical analysis, inversion, wavelets, and probabilistic and statistical approaches are used for studying thin beds. For validation, either synthetic data, core-derived analysis or other available observations are used. In this work, fuzzy membership functions are developed to represent the volume of investigation of well-logs. They are verified to model geological beds that are thinner than the vertical resolution of logging tools. The volumetric Nyquist frequency, which is suitable for volumetric measurements, e.g. well-logs, is developed. Regression models are provided to deconvolve well-logs to better interpret geological thin-beds. For validation, synthetic and core data are used.

2. Geology and log characteristics of the Sarvak Formation

The data available for this study come from the carbonate Sarvak Formation, through two exploratory oil wells (#1 and #3) in an oilfield in the Abadan Plain, Iran (see table 1). The type section of the Sarvak Formation (thickness of 832 m) is in Bangestan Mountain, Khuzestan Province, Iran. It is a hydrocarbon-producing formation with many oilfields in the Zagros Basin. Sarvak mostly overlies the Kazhdumi Formation and is overlaid by the Ilam Formation (Ghazban 2009). However, in the field under study, there is an eight metre-thick Laffan Formation between Ilam and Sarvak (figure 1).

The Sarvak Formation is a homoclinical carbonate ramp, deposited from Albian to Turonian (Mehrabi *et al* 2015). In homoclinical carbonate ramps, there is a slight seabed dip towards the sea. This term belongs to a topological classification of carbonate ramps (Read 1985). The lithology of Sarvak is wackestone–packstone. The upper Sarvak belongs to a shallower environment, compared to the pelagic facies of the middle and lower Sarvak (James and Wynd 1965 and Ghabeishavi *et al* 2010).

From the viewpoint of sequence stratigraphy, four sequences of the third order (duration of 1.5–3 Ma and thickness of 50–150 m) are distinguished in the Sarvak. Several sequences of the fourth and fifth order are also reported (Razin *et al* 2010 and Vincent *et al* 2015).

There is a depositional gap at the top of Sarvak (Cenomanian unconformity, figure 1), which improved the reservoir quality of the upper Sarvak. In most regions, vuggy porosity, karstification and bauxite mineralization are consequences of the depositional gap (Zarasvandi *et al* 2008).

3. Three types of vertical resolution in well logging

The resolution of well-logs can be investigated vertically and horizontally. Horizontal resolution is equivalent to the depth of investigation, and vertical resolution can be categorized into three types: (i) sampling rate, (ii) vertical resolution of tool (VRT) or spacing and (iii) vertical resolution of membership function (VRmf), which is introduced here for the first time. VRmf is representative of the whole effective interval on the recording, and is in the domain of the membership function. We will show that the VRmf is not necessarily the same as the spacing. The depth of investigation and VRT available for this study are presented in table 2.

The concept of the synthetic-log defined here in the synthetic cases is equivalent to the well-log in real datasets. The definition of the ideal-log in synthetic cases is equivalent to the real-log in real datasets. Hence the synthetic-log is an approximation of the ideal-log, whereas the well-log is an approximation of the real-log.

4. Basics of membership function of log records

Although a volumetric response is acquired, figure 2(a), the recorded value is conventionally assigned to the centre of the volume of investigation, i.e. the volumetric nature of the recording is ignored. The fuzzy membership function is used here to disclose the contribution of each level (or depth) to the recorded well-log value. The membership function is designed according to the mechanism of each instrument.

Well-logs can be categorized into two types: passive and active. Passive logs are simple recordings of a specific wellbore property, and can be created by a single recorder, e.g. recording natural GR through the formation. However, active logs require a transmitter or source of energy (e.g. electromagnetic, DT, beam, etc) to stimulate the formation and record the response through a set of receivers, figures 2(b) and (c).

In passive logs, the depths that are closer to the recorder have more effect on the well-log value. The membership function has to be symmetric and its height must be exactly at the level of the detector. Designing a membership function involves two stages. In the first stage, a membership function

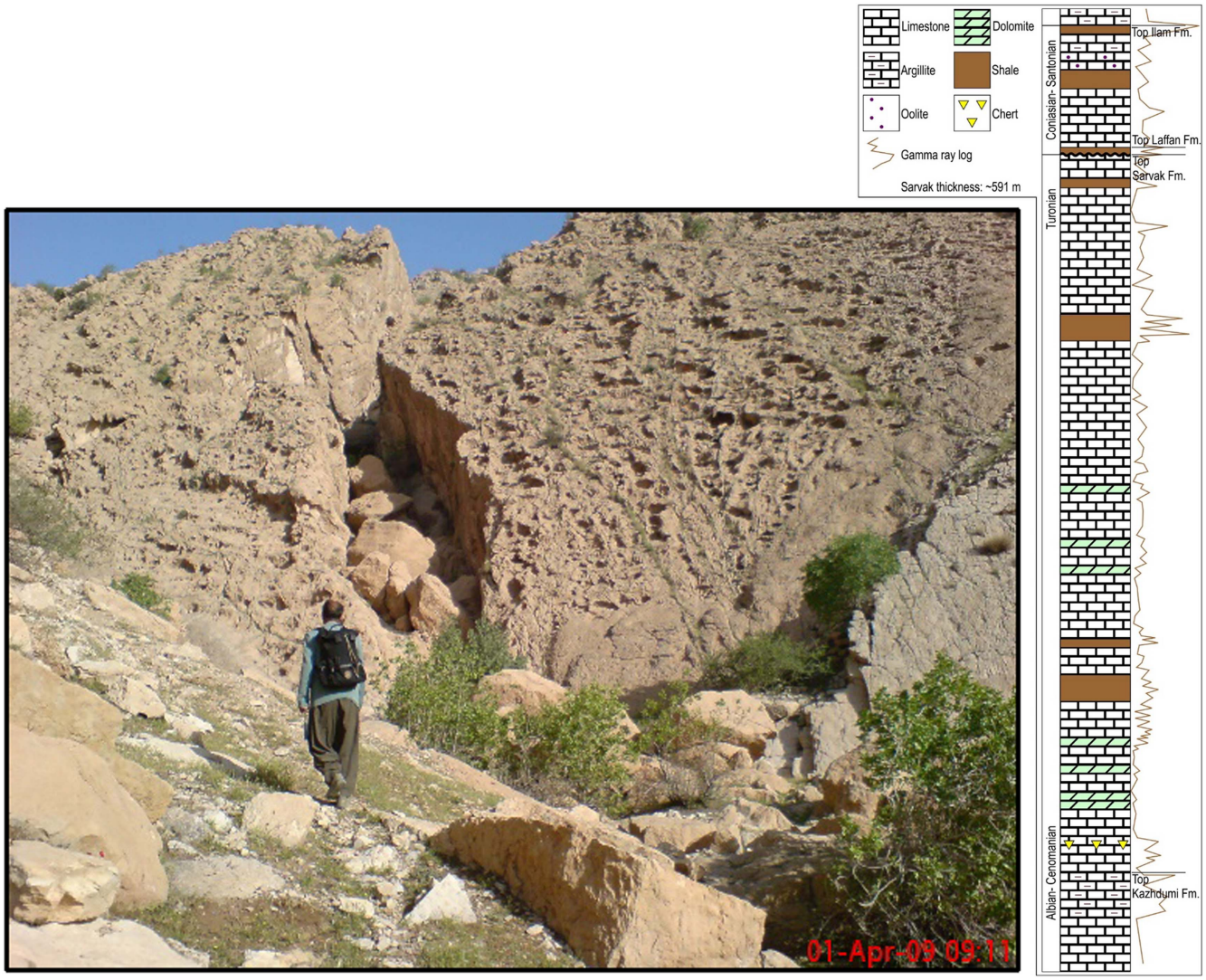

Figure 1. (a) Vugs on the top of Sarvak, Kabir-Kuh anticline, Lorestan province, Iran. (b) Lithostratigraphy of the Sarvak Formation and its neighbours, well#3, the Abadan Plain, Iran.

is assigned to each transmitter (or receiver). The simplest possible fuzzy membership function, the triangular one, figure 2(b), is used. Using non-linear membership functions will result in complex models, and since simple models work, it is not necessary to develop complex models. The membership function is more complex in active logs. Figure 2(c) shows two triangular membership functions. The height of one of them is maximized exactly at the transmitter level (mfT), while the height of the other is at the receiver (or the centre of multiple receivers) level (mfR). Recording takes place at the receiver(s), but both mfT and mfR are required for recording. Therefore, an intersection operator, here the minimum, is necessary to fuse mfT and mfR to calculate the final membership, solid line in figure 2(c).

The domain of the triangle (or VRmf) is the only unknown parameter in membership functions (figure 2). The domain was first set as spacing between the transmitter and the receiver(s) (table 2). Designing a well-log simulator based on this assumption results in the generation of abnormally high frequencies in synthetic-logs. This could be related to: (i) the incompatibility of the VRmf with the spacing (table 2), or (ii) smoothing algorithms (noise reduction or up-scaling) in the pre-processing stages. Up-scaling techniques are used to match the standard sampling rate (15.24 cm). So, an approximation of VRmf is required.

5. Estimating VRmf

To estimate the VRmf, we first check the well-logs manually. It is understood that 5, 8 or 12 continuous records (for GR, NPHI and RHOB logs) are required to have a complete response (bell shape) for the thinnest detectable beds within a homogeneous host rock. For a specific geological setting, the well-log shape is controlled by: (i) the volume of investigation, (ii) the sampling rate and (iii) the configuration of the recording points relative to the thin-bed. The effect of the configuration of the nodes on well-logs is shown in figure 3.

Table 2. Accuracy, depth of investigation and vertical resolution of logging tools (Schlumberger 2015).

Well log	Accuracy	Depth of investigation (cm)	Vertical resolution of tool (spacing) (cm)
GR	±5%	60.96	30.48
RHOB	±0.01 g cm^{-3}	12.70	45.72
NPHI	0–20%: ±1% 20–30%: ±2% 30–45%: ±6%	~23	30.48
DT	±6.6 $\mu s\ m^{-1}$	7.62	91 152

Two different configurations result in two different well-logs. In configuration A (figure 3, solid line), only one point detects the thin bed, and it is strongly affected by it. In configuration B (figure 3, dashed line), there is no detection within the thin-bed, and the bed has only a minor influence on the two nearby records. So, there is a balance between the amplitude and the apparent thickness. Furthermore, this balance is used to model the real thickness and petrophysical values of the thin-beds.

The larger the intersection of the volume of investigation (or VRmf) of adjacent records, the greater the similarity between neighbouring records. When the continuity increases, the well-log becomes smoother. To study the similarity of the neighbouring records, the correlation coefficient is first checked between pairs of neighbouring records (R_i, R_{i+j}). R_i is the ith record, and R_{i+j} is the jth neighbour of R_i. As an example, in the GR log of well#2, the correlation coefficients between the neighbours ($j = 0$, 1, 2, 3, 4 and 5) were 100%, 93%, 81%, 70%, 62% and 57%, respectively. This shows mathematically that the similarity between the neighbouring records reduces as the distance increases between the pairs of records. A correlation coefficient of more than 90% can be considered as very high correlation, and 70%–90% as high correlation (Mukaka 2012). Considering the cut-off for high correlation (>70%), which corresponds to high similarity, three neighbours ($j = 3$) will be highly similar to each other. So, for GR in well#2, the VRmf contains three adjacent records ($j = 1$, 2, 3), but not the fourth, i.e. $3 \times 15.24\,\text{cm} < \text{VRmf} < 4 \times 15.24\,\text{cm}$ or $46\,\text{cm} < \text{VRmf} < 61\,\text{cm}$. Although the correlation coefficient provides an approximation for the VRmf, variography analysis is viewed as being preferable, because variography is a specialized tool to quantify the variability (including continuity) of spatial data (Gringarten and Deutsch 2001).

Experimental variographs of well-logs are checked for five available wells within the Sarvak reservoir, SW Iran. There is an exact linear relation at small lags in all the wells (figure 4). There is no nugget effect, i.e. all the variographs start from about the centre of coordination (0, 0). The nugget effect and the initiation of variographs are measures of discontinuity (Gringarten and Deutsch 2001). So, the first structure, which is linear, is considered as a cut-off of high similarity between neighbouring records. Interpreting the variograph of GR in well#2, figure 4(a), reveals that four adjacent records are very similar to each other, leading to VRmf = 61 cm, which is close to the approximation of the correlation coefficient. Hence, the linear parts of the variographs are interpreted as indicating high similarity between the records, and are representative of the VRmf for further calculations (tables 3, 4).

6. Methodology

6.1. Designing membership functions

6.1.1. Passive log: gamma ray. The GR detector belongs to the category of passive logs, since it only records the released energy of radioactive elements such as uranium (U), thorium (Th) or potassium (K) within the formation. New GR recording tools can distinguish the source elements (U, Th or K) based on the detected ray's level of energy. Therefore, the triangular membership function mfD is suitable to show the contribution of each horizon to the recorded value, figure 2(b). The VRT of GR is 30.48 cm, while its VRmf is 61 cm (table 4).

6.1.2. Triangular active logs: bulk density and neutron porosity. RHOB belongs to the active log category, and has a transmitter and a receiver simultaneously. It transmits GR toward the wellbore and records its attenuation (Dewan 1983). Therefore, a triangular membership function min{mfT,mfR} is suitable to show the contribution of each horizon to the recorded value, figure 2(c). The VRT of RHOB is 45.72 cm and its VRmf is 76 cm (table 4).

Like the RHOB, NPHI is an active log. It transmits fast neutrons (~5 meV) in all directions and records very low or thermal energies (~0.025 eV) (Dewan 1983). Therefore, the membership function min{mfT,mfR} represents the contribution of each horizon to the recorded value, figure 2(c). The VRT is 30.48 cm and the VRmf is 76 cm in the NPHI log (table 4).

6.1.3. Complex active log: sonic. For DT, defining the membership function is not as simple as it was for the previous logs, since the borehole compensated (BHC) sonic tool has two transmitters on each end part and four detectors (figure 5). The BHC measures the transmitting time twice, one measurement relates to the top transmitter and the other relates to the bottom transmitter. In addition, each transmitter is linked to a pair of detectors in order to apply wellbore-related corrections to remove the effect of mud filtrate. Finally, the two transmitting times are aggregated by an averaging operator to (i) increase the signal-to-noise ratio and (ii) make the final log more symmetric.

The membership functions for the transmitters (mfT1 and mfT2) and detectors (mfR1A, mfR1B, mfR2A and mfR2B) are set to be linear, figure 5(a). The minimum operator is used to create four membership functions (two for each half) between each transmitter and linked detectors. The membership functions mfDT1A and mfDT1B (mfDT2A and mfDT2B), which relate to the top (bottom) transmitter, are averaged to produce mfDT1 (mfDT2). These created

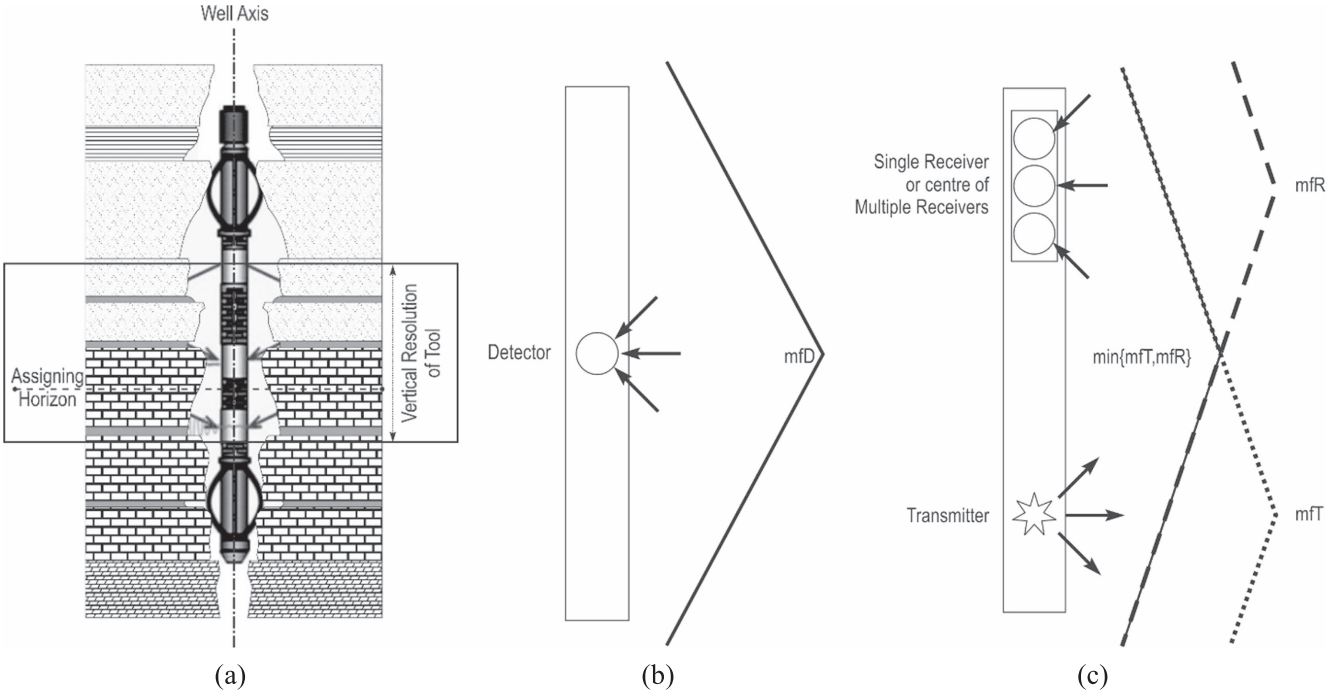

Figure 2. Schematic representations of tools for recording well-logs (a). Rough fuzzy membership functions of horizons around the detector (s) and transmitter are shown for (b) passive and (c) active logs.

membership functions are fused by an averaging operator to produce the final membership function of DT, mfDT in figure 5(b). Practically, mfDT is not useful since the VRmf is estimated to be 61 cm (table 3), while the VRT is 152 cm. So mfDT is rescaled to become valid for synthetic-log simulation, figure 5(c). The properties of the defined membership functions are used to generate synthetic-logs for thin-bed characterization (table 4).

6.2. Volumetric Nyquist frequency

The relation between the sampling rate (SR) and the VRmf can be categorized into three types: (i) VRmf $= 0$, (ii) $0 <$ VRmf $<$ SR and (iii) SR $<$ VRmf. The physical difference between categories (i) and (ii) is shown in figures 6(a) and (b). The Nyquist frequency is developed in telecommunication systems (Nyquist 1924) where datasets are not volumetric, i.e. VRmf $= 0$, figure 6(a). Well-log datasets have the nature of categories (ii) and (iii), figures 6(b) and (c). The famous Nyquist frequency is conventionally used in well-log interpretation, and a modification of this concept is presented here.

In the case of VRmf $= 0$, when the thickness of a geologic bed exceeds that of the SR, it is certain that at least one record will detect the bed: a probability of one, see the solid line in figures 7(a) and (b). The chance of detecting this bed decreases linearly as its thickness decreases to zero: see the linear part of the solid line in figures 7(a) and (b).

When VRmf > 0, the thickness of the bed must exceed the summation of SR + VRmf to be certain that the bed will occupy the whole volume of investigation of at least one record: a probability of one, see the dotted and dashed lines in figures 7(a) and (b). As before, the thinner the bed, the smaller the probability of detection: see the linear parts in the dotted and dashed lines in figures 7(a) and (b).

In the literature, a belief function indicates lower probability, and presents a pessimistic view of the chance of something happening (Dempster 1967 and 1968). From figures 7(a) and (b), we see that the probability function for detecting a bed that is thinner than the SR is linear, whereas the belief function is zero: see the solid line in figures 8(a) and (b). When $0 <$ VRmf $<$ SR, the belief function shows a fuzzy relation. When the bed is thicker than SR + VRmf, it is certain that the volume of investigation of at least one record will be completely affected by the bed. Finally, when the bed is thinner than the VRmf, only some parts of the volume of investigation can be influenced by the bed.

Consequently, the conventional Nyquist frequency is not completely effective in volumetric recordings, like well-logs. When VRmf > 0, beds thinner than VRmf cannot be detected without the shoulder-bed effect. To be certain of detecting a bed in non-volumetric measurements, the thickness of the bed has to be at least equal to that of the SR, but for volumetric measurements, the thinnest certainly detectable bed without the shoulder effect is SR+VRmf. The range of uncertainty thus remains constant for all three categories (table 5). Based on descriptions, if relation (1) is considered as a definition of the volumetric Nyquist frequency ($fr_{\mathrm{Nq,vol}}$), table 5 can be reconstructed for all the categories: VRmf $= 0$, $0 <$ VRmf $<$ SR or VRmf $>$ Sr

$$fr_{\mathrm{Nq,vol}} = \frac{1}{\mathrm{SR} + \mathrm{VRm}f}. \qquad (1)$$

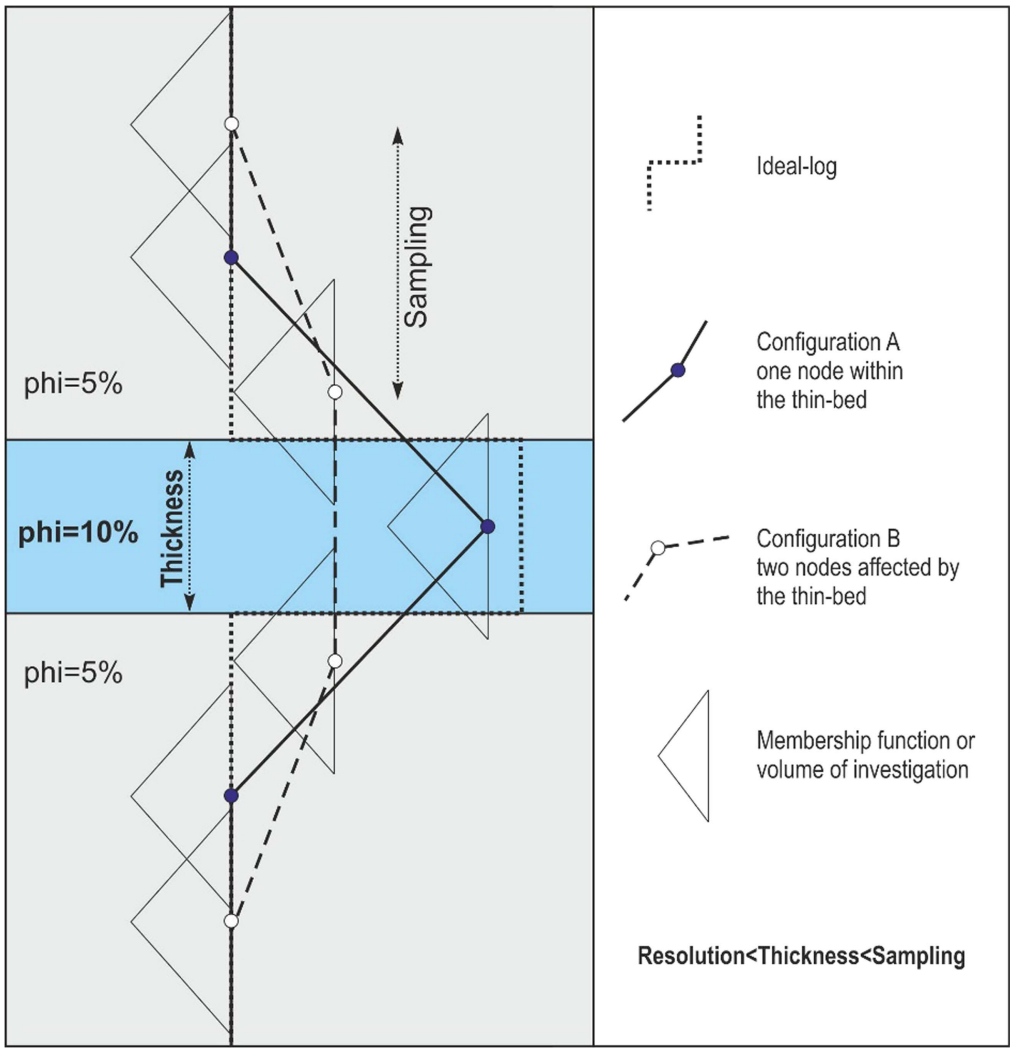

Figure 3. Two possible configurations for detecting a thin-bed.

6.3. Geometric thin-bed modelling

6.3.1. Scale of the modelling. The thickness target in the current paper is limited to moderately thin and thin-beds, as introduced by Majid and Worthington (2012), regarding log responses: thick, moderately thin (10–60 cm), thin (3–10 cm), very thin (1–3 cm) and laminated (0.1–1 cm). There is no thin-bed problem in thick-beds because the thickness allows logging instruments to measure the real petrophysical properties without the shoulder-bed effect. This means that the thickness of a thick-bed is not smaller than the vertical resolution of the tool. A moderately thin-bed is defined as detectable, pluggable (i.e. it can be cored) and identifiable, while the well-log cannot show the real petrophysical value of the bed, i.e. the thickness is smaller than the spatial resolution. The thickness of a thin-bed is much smaller than the vertical resolution, but it is pluggable and identifiable. A very thin-bed is not pluggable but can be identified by micro-imaging devices and certain meso-scale tools (indirectly). A laminated-bed (below the scale of a centimetre) cannot be identified, even by micro-imaging devices.

6.3.2. Thin-bed simulator. Consider a thin-bed with a petrophysical value of q_2, located between two thick-beds, with petrophysical values of q_1 and q_3, figure 9(a). Due to the shoulder-bed effect, it is anticipated that the value of the recorded log will be a weighted average of q_1, q_2 and q_3. The weights have to show the degree of each bed's contribution to the recording. It is expected that q_1 will have a larger weight if it occupies more space within the volume of investigation compared to q_2 and q_3 (figure 9(b)).

Based on the introduced membership functions, a simulator is devised to generate synthetic-logs for the GR, RHOB and NPHI of the thin-bed. Due to the complexity of the membership function, the DT simulator is not designed here. To create a synthetic-log for a triangular membership function, all the configurations have to be considered, figure 9(a). In order to limit the number of configurations to

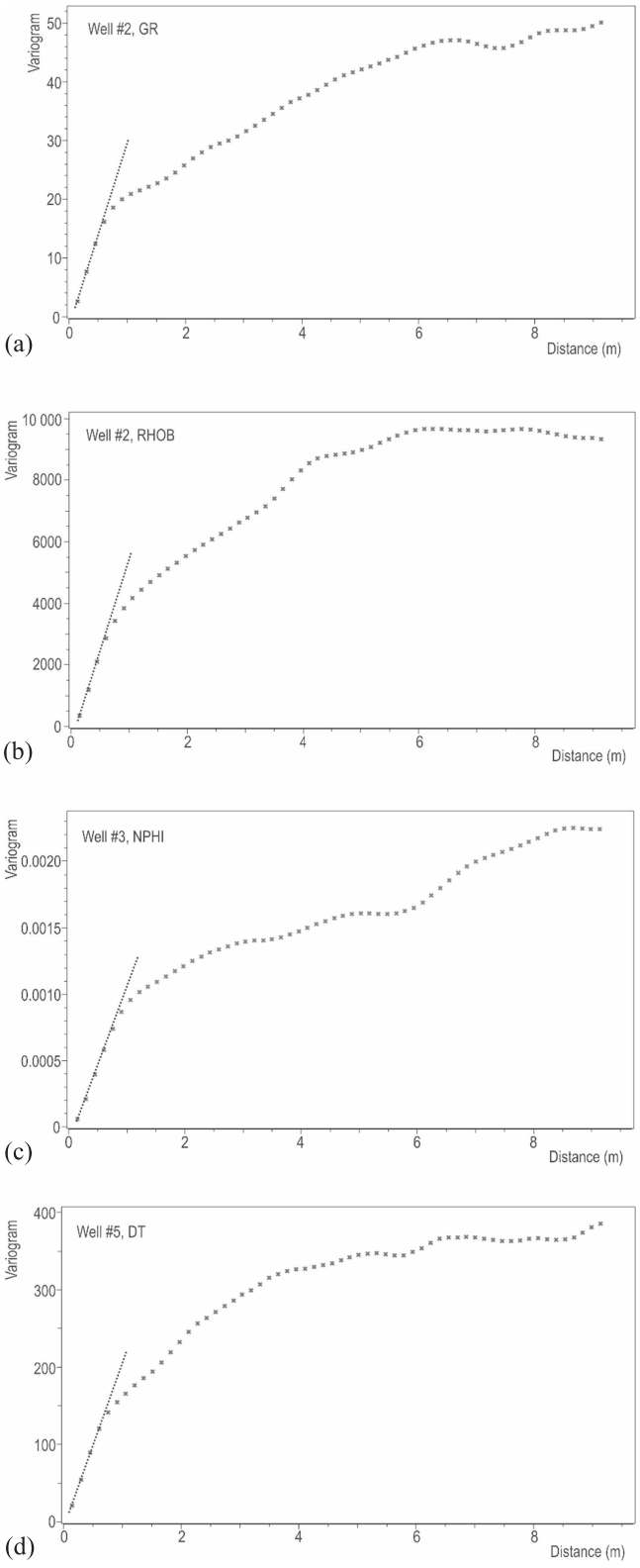

Figure 4. Experimental variographs showing a linear relation at the first lags. An open-source computer package called Stanford Geostatistical Modeling Software (SGeMS) is used to generate the variographs. (a) GR in well#2, (b) RHOB in well#2, (c) NPHI in well#3 and (d) DT in well#5.

seven, figure 9(a), the thickness of the thin-bed should be less than half of the VRmf.

In the next step, the theoretical formula of a synthetic-log is calculated for each configuration. The calculations are based on geometric analytics (figure 9(b) and appendix A). The synthetic log $\mathrm{s\,log}(z)$ is the integral of the petrophysical values $q(x)$ multiplied by the membership function $\mathrm{MF}(x)$ over the VRmf

$$\mathrm{s\,log}(z) = \int_{\frac{z-\mathrm{VRmf}}{2}}^{\frac{z+\mathrm{VRmf}}{2}} q(x).\,\mathrm{MF}(x).\,\mathrm{d}x. \tag{2}$$

To compute $\mathrm{s\,log}(z)$, convolution relation (2) can be written discretely. The convolution form of relation (2) is shown in appendix B. The volume of investigation is divided into four parts, figure 9(b): S_1 to S_4, and the ratio of S_i to $\sum_{i=1}^{n} S_i$ is defined as the weight of each q_i for averaging (relation (3))

$$\mathrm{slog}\left(\tfrac{n+1}{2}\right) = \frac{\sum_{i-1}^{n} q_i \,.\, S_i}{\sum_{i-1}^{n} S_i}$$
$$= \frac{1}{\sum_{i-1}^{n} S_i} \,.\, (q_1 \,.\, S_1 + q_2 \,.\, S_2 + \ldots + q_n \,.\, S_n). \tag{3}$$

The limitations of using relation (3) are: (i) the existence of a thin-bed between two thick-beds, (ii) the wellbore is perpendicular to geological beds, (iii) $q_1 = q_3$ (single thin-bed limitation), (iv) triangular membership function and (v) the thickness of the thin-bed $\leqslant \frac{1}{2}\mathrm{VRmf}$.

S_1 and S_4 are triangles, and S_2 and S_3 are trapezoids, figure 9(b). *hb* and *ht* are the distances from the centre of the VRmf to the bottom and top of the thin-bed, respectively. Because all the depths are known, *hb* and *ht* are also known variables; *at* and *ab*, figure 9(b), can be calculated by *hb*, *ht* and the height (=1) by means of the intercept theorem of Thales. The same weights are calculated for other configurations, and are presented in appendix A

$$at = 1 - \frac{2.ht.1}{\mathrm{VRmf}}, \tag{4}$$

$$ab = 1 - \frac{2.hb.1}{\mathrm{VRmf}}. \tag{5}$$

6.3.3. Thin-bed deconvolution relations. It is necessary to deconvolve well-logs (here GR, RHOB and NPHI) to characterize a thin-bed accurately, i.e. decrease the shoulder-bed effect to approximate the real thickness and the real petrophysical value of a thin-bed. Here, thin-bed deconvolution is based on the balance between the amplitude and apparent thickness of the well-log (figure 3), thus a statistical analysis is used to find a relation between the

Table 3. Finding the VRmf for each well-log in each well using variography analysis. The data are from the Sarvak Formation, Zagros. The VRmf is selected as the minimum value within all the wells because larger values might be related to the homogeneous media of the rocks. Units: cm.

Well log	Well #1	Well #2	Well #3	Well #4	Well #5	VRmf
GR	61	61	61	61	61	**61**
RHOB	76	76	91	76	76	**76**
NPHI	76	76	91	76	76	**76**
DT	61	61	61	61	61	**61**

Table 4. Specifications of designed membership functions for each well-log.

Well log	Vertical resolution of tool (VRT) (cm)	Type of membership function	Vertical resolution of membership function (VRmf) (cm)	Height of membership function
GR	30.48	triangular	61	middle
RHOB	45.72	triangular	76	middle
NPHI	30.48	triangular	76	middle
DT	152.00	complex	61	15 cm in the middle

synthetic- and ideal-logs. To develop deconvolution relations, a set of ideal-logs is first generated. This means that the petrophysical specifications of the thin-beds (thickness of the thin beds and values of q_1, q_2 and q_3) have to be defined. Five thicknesses are assumed: 5, 10, 15, 20 and 30 cm. Due to the limitations of the model in the previous section, it is assumed to have the same petrophysical values above and below the thin-bed, i.e. $q_1 = q_3$. Without loss of generality, we assume that $q_1 = q_3 = 0$, because the goal is to rescale or deconvolve the shape of the well-log, i.e. reduce the shoulder-bed effect. Therefore, only the relative values of q_2 to q_1 (or q_3), before and after imposing the shoulder-bed effect are important. The petrophysical value of q_2 is set to be 1, 3, 5, 7, 10, 12, 15, 17, 20, 22, 25, 27 or 30 for GR (API) and NPHI (%), whereas it is considered to be 0.01, 0.02, 0.05, 0.07, 0.10, 0.12, 0.13 or 0.15 for RHOB (g cm^{-3}). Recall that these values are not absolute petrophysical values. They are the relative differences of the thin-bed petrophysical specification according to the upper and lower beds. Combining the thickness and petrophysical values of the synthetic thin-beds, 65 ideal-logs for GR and NPHI, and 40 ideal-logs for RHOB, are generated.

In the second stage, the log simulator is run over the ideal-logs. Synthetic-logs are the results of convolution (relation (2)), hence contaminated by the shoulder-bed effect, figures 10(a) and (b). The crosses on figure 10(a) are synthetic-log values plotted against ideal-log values. All the values are below the line $y = x$, i.e. underestimated by the synthetic-log. The thickness of the thin-bed read from the synthetic-log is plotted against the thickness read from the ideal-log, crosses in figure 10(b). The crosses above the line $y = x$ are thickness overestimations. The underestimation of the petrophysical value and the overestimation of thickness is expected because of the nature of the shoulder-bed effect.

For figures 10(a) and (b), the regression lines are calculated (relations (10) and (11)). The same relations are given for GR and RHOB synthetic logs (relations (6)–(9)). The inputs for the regression models are thickness and the relative well-log (or synthetic-log) value for the thin bed, and the outputs are regression models, representing the real thickness (or ideal thickness) and the relative real-log (or ideal-log)

$$\Delta GR_{reg} = 1.0356\ \Delta GR_{log} + 0.0669\ TH_{log\ GR}, \quad (6)$$

$$TH_{reg} = -0.1663\ \Delta GR_{log} + 0.2926\ TH_{log\ GR}, \quad (7)$$

$$\Delta RHOB_{reg} = 0.9127\ \Delta RHOB_{log} + 0.0007\ TH_{log\ RHOB}, \quad (8)$$

$$TH_{reg} = 115.591\ \Delta RHOB_{log} + 0.1860\ TH_{log\ RHOB}, \quad (9)$$

$$\Delta NPHI_{reg} = 1.0262\ \Delta NPHI_{log} + 0.1124\ TH_{log\ NPHI}, \quad (10)$$

$$TH_{reg} = 0.7417\ \Delta NPHI_{log} + 0.1499\ TH_{log\ NPHI}, \quad (11)$$

where TH stands for thickness. For the GR model, the thickness, read from the well-log, has to be thinner than 100 cm, and the difference of the well-log value of the thin-bed, relative to the upper and lower beds, should be lower than 30 API. The acceptable domain of thickness for RHOB is up to 110 cm, and the maximum relative well-log value is 0.15 g cm^{-3}. The NPHI of the thin-bed can vary by 30%, figure 10(a), and its well-log-based thickness should be thinner than 110 cm, figure 10(b).

Finally, the developed relations are applied to the outputs of simulators (i.e. synthetic-logs) to move (map) the crosses closer to $y = x$, i.e. for better matching to the ideal-logs, dots in figures 10(a) and (b). Based on the MSE of the synthetic data, the error in characterizing petrophysical values is reduced two to three times and the error in the thickness estimation is reduced 40 to ~80 times (table 6).

7. Results and discussion: case-study for thin-bed characterization

Deconvolution relations (6)–(11) are applied to real well-log data, within the interval of the carbonate Sarvak Formation, through two exploratory oil wells in the Zagros Basin, Iran.

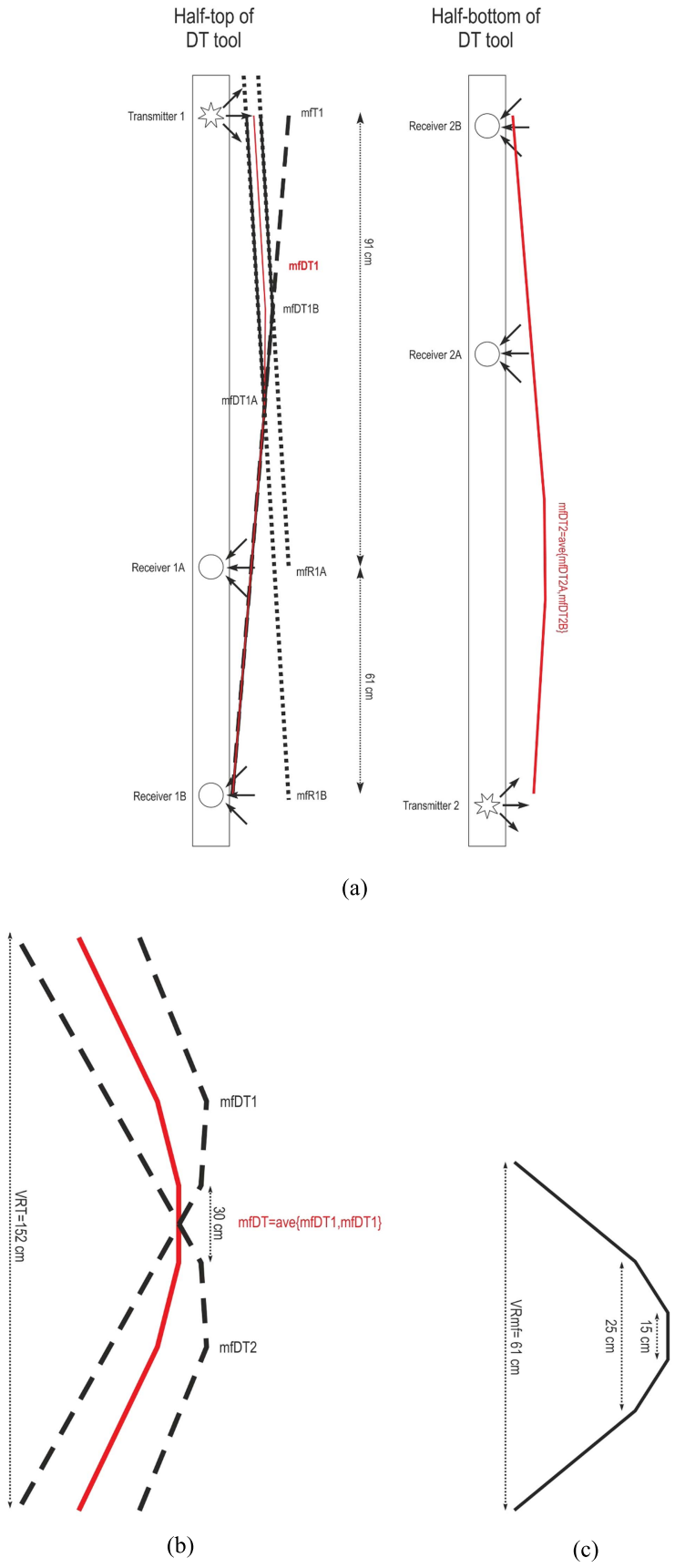

Figure 5. Designing the membership function for DT. (a) Defined membership function for each half-part of the sonic tool (figure 1(c), table 2). mfDT1A = min{mfR1,mfT1A}, mfDT1B = min{mfR1,mfT1B} and mfDT1 = ave{mfDT1A,mfDT1B}. (b) Theoretical membership function based on the VRT. (c) Final membership function by scaling the VRT to the VRmf.

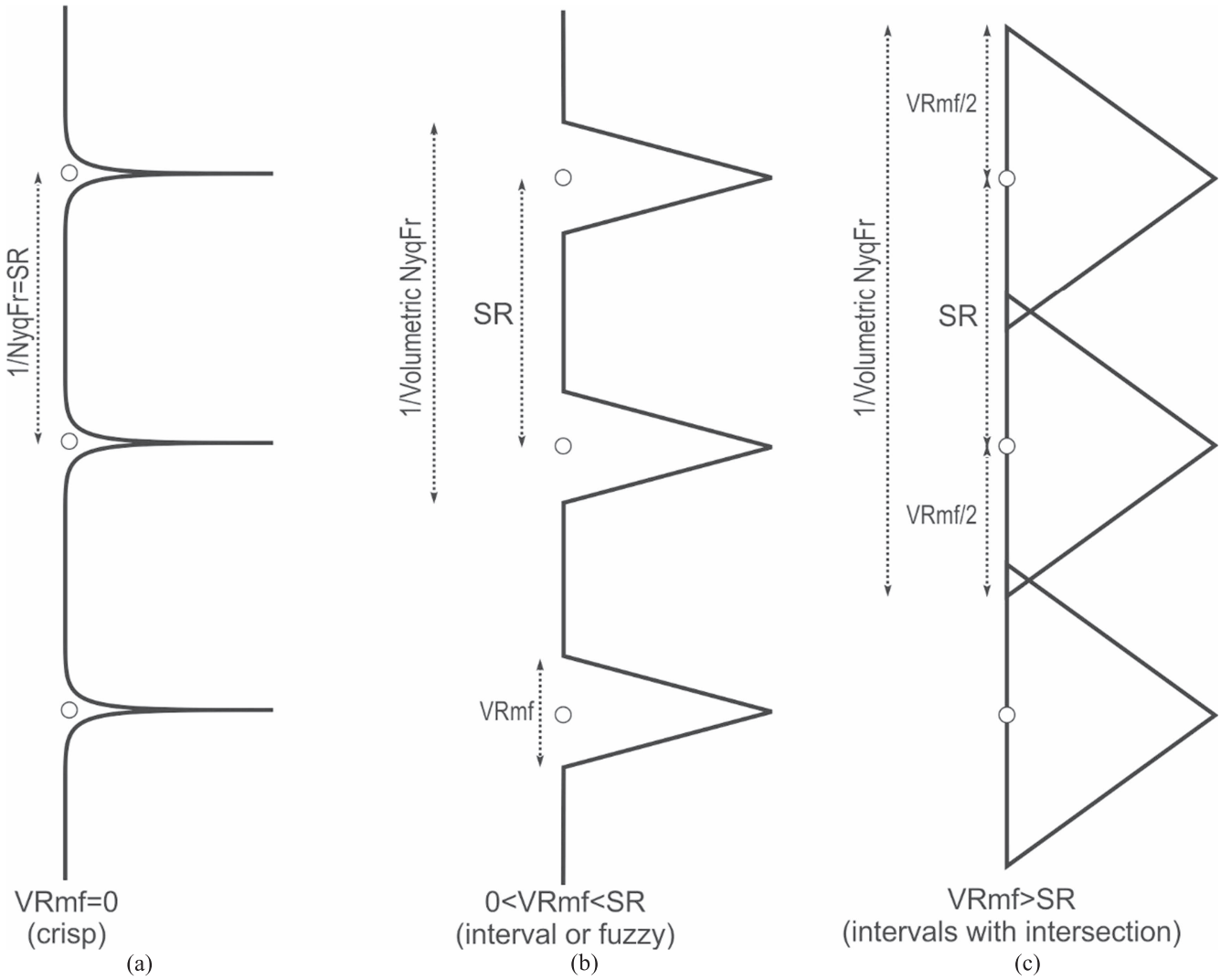

Figure 6. Nyquist frequency in three categories. Small balls are recording centres. (a) Pulse shape (VRmf = 0), like datasets in telecommunications in the time domain. (b) Detections with volume of investigations (VRmf > 0) but VRmf < SR. (c) When there are intersections between the volume of investigations of adjacent records (VRmf > SR).

First, the authors selected ten points through well#1 that represent the behaviour of a thin-bed, i.e. there are small simultaneous peaks in two or three well-logs (GR, RHOB and NPHI) (table 7).

It is worth mentioning why the observations of table 7 and figure 11 are interpreted as thin-beds. Very thin-beds that do not have any effect on the well-logs are of course undetectable in the well-scale. When the beds have some effects on two or three well-logs, there are two possibilities. (i) The bed is thick enough to let the receivers detect its real petrophysical values, i.e. the shape of the well-log is stable, not a peak or a trough. (ii) The bed is so thin that only a few records can reflect it (configurations A or B, figure 3). In this case, the well-log shows a peak or a trough shape, and cannot fully represent the real petrophysical values. So, when there are peaks or troughs at the same depth within well-logs, they are interpreted to be thin-beds. They could also be interpreted as geological phenomena other than thin-beds, e.g. vuggy or fractured intervals. The former interpretation is correct, because in the petroleum industry well-logs are acquired within sedimentary deposits where the geological phenomena are located.

Then, the thickness and variation of the petrophysical values are measured from well-logs and added to table 7. These values are far from the real thickness and petrophysical values due to the shoulder-bed effect. Now, using relations (6)–(11), the shoulder-bed effect is reduced to get closer to the real values (table 7).

In practice, a thin-bed has to be characterized by different logs individually, with the results being combined together to lead to a final decision on the estimation of the thickness and real-log values. The main reason for this is the fact that a thin-bed might show a specific change in a petrophysical parameter, e.g. in a highstand systems tract (HST), the GR might show meaningful variations of sea level, whereas the other logs do not. Therefore, using various logs simultaneously will not necessarily lead to a successful thin-bed characterization. Because of the difference in the volume of investigation and the sampling rate of well logs, thin beds are also better investigated individually. This method of thin-bed

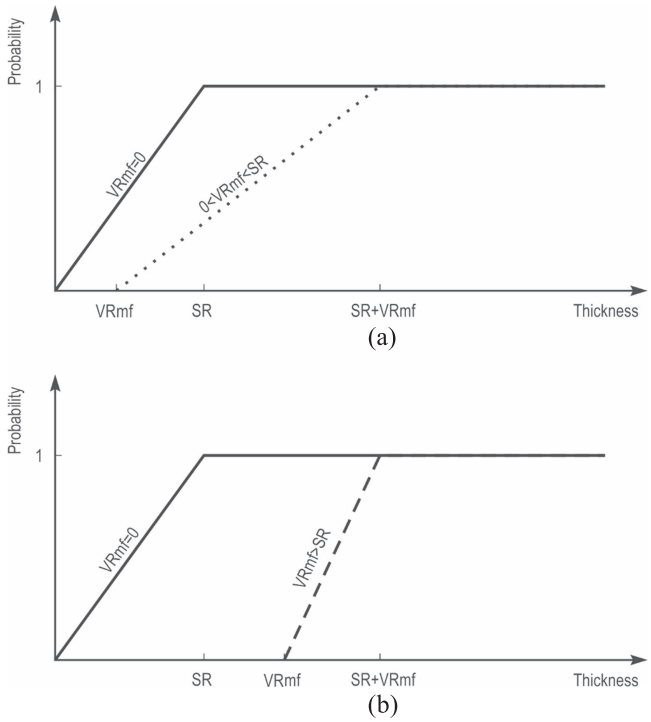

Figure 7. Comparison of the probability of detecting the real petrophysical value of thin-beds, i.e. without the shoulder-bed effect, for the three categories. When VRmf = 0, solid lines in (a) and (b), the common Nyquist frequency is effective, i.e. the SR is the minimum detectable thickness of a thin bed. (a) VRmf < SR, dotted line. (b) VRmf > SR, dashed line.

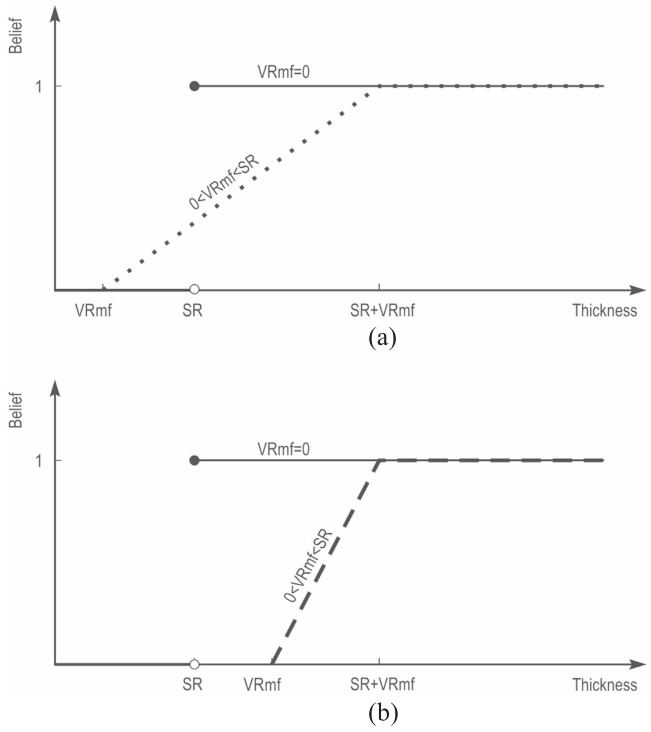

Figure 8. Comparison of the belief function (pessimistic view) for detecting the real petrophysical value of thin-beds, i.e. without the shoulder-bed effect, for three different sensor types. When VRmf = 0, solid lines in (a) and (b), the common Nyquist frequency is effective, i.e. the SR is the minimum detectable thickness of a thin-bed. (a) VRmf < SR, dotted line. (b) VRmf > SR, dashed line.

characterization has been addressed in the literature (Gallet and Courtillot 1989, Desvignes *et al* 1992 and Heidari *et al* 2012).

The application of deconvolution relations (6)–(11) amplifies all the petrophysical values. In eight observations (#1–4, #6–8 and #10), three thickness models can be given (relations (7), (9) and (11)), and in two observations (#5 and #9), only two thickness models can be obtained (relations (7) and (11)). The final thickness is calculated by a weighted average of the thickness models, with regard to the $\sqrt{\text{MSE}}$ of each model (table 6). The standard deviation of the thickness values shows similar values in nearly all of the cases. Hence, fusing three thickness models increases the confidence level of thickness value.

In observation#3, for example, according to the GR model, the thickness is 22.48 ± 7.12 cm (table 7). The thickness derived from the RHOB model is 25.10 ± 8.20 cm, which is just a little thicker, although the GR model is more precise. The third thickness value estimate (16.67 ± 7.30 cm), given by the NPHI model, is lower than the others. The final thickness value is the weighted average of the three values provided by the thickness models. The final thickness for observation#3 is 21.42 ± 7.57 cm. White noise can be reduced through fusing multiple outputs. The standard deviation of the three thickness values (22.48, 25.10 and 16.67 cm) is very small (3.52 cm) compared to the final error of the estimate deduced from $\sqrt{\text{MSE}}$ (7.57 cm) (table 7).

Based on the concept of the volumetric Nyquist frequency, there is no guarantee of having a direct measurement of a thin-bed that is thinner than SR + VRmf (relation (1)). However, a deconvolution procedure based on a geometric simulator is developed, which is able to estimate the petrophysical and thickness values of thin-beds that are thinner than SR + VRmf after reducing the shoulder-bed effect. The thin-bed characterization after deconvolution is much more accurate (table 6). The characterization results for ten thin-beds (thickness values from 14 to 30 cm, table 7) are promising for the development of the methodology for other well-logs. The well-logs for the thinnest characterized bed, observation#7 (table 7), are provided and interpreted, figure 11(a).

At a depth of about 3158.19 m, there are positive peaks in the GR and NPHI logs, and there is a negative peak in the RHOB. The GR increase is due to shale content (here the GR log is only the response of the potassium content). The increase of the NPHI at this depth is a sign of increased total porosity. The decrease of the RHOB could be related to the simultaneous increase of the porosity and shale content. The RHOB log around this horizon fluctuates between 2.71 g cm^{-3} (equivalent to the density of calcite) and 2.65 g cm^{-3} (equivalent to the average density of shale) (Ellis and Singer 2007). So, this thin-bed can be interpreted as a shale inter-layer with a thickness of 15.0 ± 7.5 cm, figure 11(a). The error (±7.5 cm) is calculated using the error propagation methodology, and is close to the expected error of ±7.75 cm, derived from $\sqrt{\text{MSE}}$ (table 7).

Table 5. Minimum thicknesses for a thin-bed to be detectable. The range of uncertainly shows the difference between the lengths that are probably and certainly detectable in each case.

	VRmf = 0	VRmf < SR	VRmf > SR
Minimum required thickness for a bed to be probably detectable without the shoulder-bed effect	0	VRmf	VRmf
Minimum required thickness for a bed to be certainly detectable without the shoulder-bed effect	SR	SR + VRmf	SR + VRmf
Range of uncertainty	SR	SR	SR

From the sedimentological viewpoint, the horizon of 3158.19 m, figure 11(a), located at the lower Sarvak Formation, belongs to the outer shelf sedimentary environment. Previous studies on this interval confirmed the deep water facies and fully marine conditions (Ghabeishavi *et al* 2010). Stratigraphic sequences of the third, fourth and fifth order were previously reported within the Sarvak Formation. Its lower part consists of about three sequences of the third order (Razin *et al* 2010 and Vincent *et al* 2015). It has the potential for lithological variation, especially increase of shale volume. Therefore, the numerical inferences about the existence and characterization of a thin-bed are acceptable (figure 11).

The thin-bed characterization method is also applied to a cored interval of upper Sarvak, within well#3, to verify thin-bed detection with the cores, figure 11(b). The lithology belongs to the shallow carbonates. According to the core porosity anomaly, 8%, figure 11(b), it is understood that the petrophysical behaviour of the black thin-bed differs from the neighbouring beds. Therefore, it might be detectable by the well-logs.

The convolution relations are applied to the NPHI and RHOB logs. The GR does not show thin-bed behaviour. The result is a thin-bed, with a thickness of 13 ± 7.5 cm, which is compatible with the black thin-bed thickness in the core box (<25 cm). It is worth mentioning that the real *in situ* thickness of the black thin-bed is smaller than that of the core box because of the weathering of cores at surface. In addition, the corrected NPHI (11.7%), which is higher than the core porosity (8%), is compatible with the fact that the effective porosity, i.e. core porosity, is never higher than the total porosity, i.e. NPHI. Since the NPHI (3.8%) is lower than the core porosity (8%), the well-log is not precise enough in thin-bed characterization.

8. Conclusion

The vertical resolution of membership function (VRmf) introduced here is a useful parameter for well-log simulation and modelling. It can be estimated using variography analysis. In five wells, the VRmf of the GR, RHOB, NPHI and DT well-logs was estimated to be 61, 76, 76 and 61 cm, respectively. Following the development of membership functions to study the volume of investigation of each well-log, it was discovered that the membership function of GR, RHOB and NPHI is triangular, while for DT it is a complex shape.

Taking the relative values of the sampling rate (SR) and VRmf into consideration, the concept of the Nyquist frequency is used in the well-logs, and a volumetric Nyquist frequency is developed for volumetric recordings (VRmf > 0). It is shown that when VRmf > 0, the minimum identifiable thickness value increases to SR + VRmf. Then a thin-bed simulator is designed using geometric relations. The simulator is used to generate numerous synthetic-logs for different geological situations. Ideal-logs (without the shoulder-bed effect) and synthetic-logs (contaminated by the shoulder-bed effect) are compared to build regression models that lead to deconvolution relations for the GR, RHOB and NPHI. They estimate the thickness of the thin-beds 40 to 80 times more accurately compared to the apparent thickness read from well-logs. Petrophysical characterization can be carried out more precisely: the $\sqrt{\text{MSE}}$ of the GR, RHOB and NPHI values was reduced from 42.25 to 20.20, 0.003 to 0.001 and 139.61 to 39.99, respectively. This methodology could be developed for all well-log data in various conditions.

Finally, the application of deconvolution relations is checked by characterizing ten real thin-beds within the Sarvak Formation. All the petrophysical values (GR, RHOB and NPHI) are increased and all the thickness values are reduced due to the decrease of the shoulder-bed effect. The resulting thickness values of the observations are calculated using a weighted average. The average standard deviation of the thickness values is 4.4 cm, which is a precise value, considering a vertical resolution of more than 60 cm.

The advantages of the geometry-based algorithm are: (i) it estimates the thickness of the thin-bed; (ii) it corrects (deconvolves) the petrophysical value of a well-log at the depth of a thin-bed; and (iii) it is easy to understand the basis of the methodology. The disadvantages are: (i) the algorithm does not provide a complete curve, i.e. the estimation only belongs to a single point, and (ii) it is time consuming and not automated.

Acknowledgments

This work was supported by the Center for International Scientific Studies and Collaboration (CISSC) and the French Embassy in Iran through the PHC Gundishapur program no. 35620UL. The authors acknowledge the Exploration Directorate of the National Iranian Oil Company for providing data and permitting the publication of scientific achievements. We

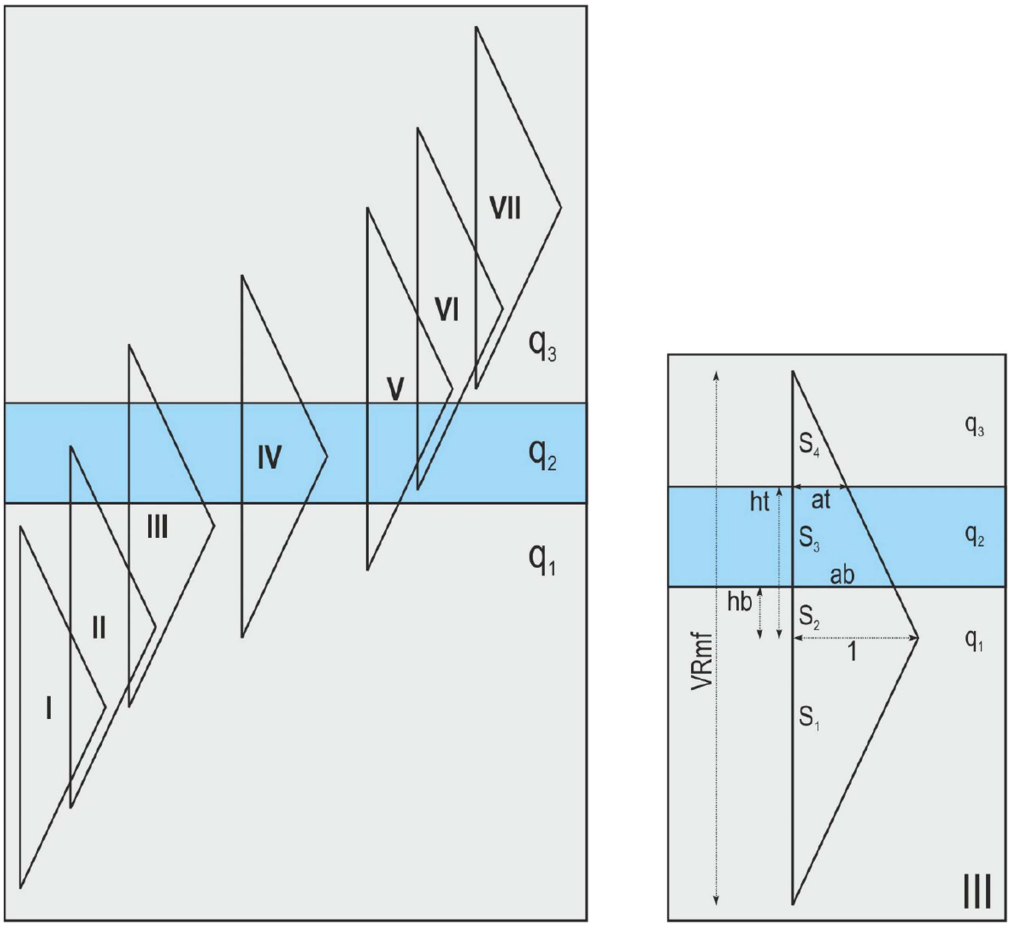

Figure 9. Considerations for generating a simulator for modelling a thin-bed. (a) Seven devised configurations (calculations are provided in appendix A). (b) Details of configuration A-3.

are indebted to the anonymous referees for their fruitful remarks, which helped improve the manuscript.

Appendix A. Simulator for each configuration

In all the calculations, the height of the membership function at the middle of the VRmf is considered as point zero of a one-dimensional (vertical) coordinate system, positive upward. Therefore, when the top (bottom) bed line is located above point zero, the value of ht (hb) is positive. And when the top (bottom) bed line is below point zero, the value of ht^{-} (hb^{-}) is negative. The negative superscript only shows the relative situation, and the sign of ht, figure 9(b). The following equations, which refer to discrete calculations corresponding to the configurations of figure 9(a), are necessary for coding.

Configuration A-1

$$\mathrm{s\,log_I} = q_1.$$

Configuration A-2

$$\mathrm{s\,log_{II}} = \frac{S_1 \,.\, q_1 + S_2 \,.\, q_1 + S_3 \,.\, q_2}{S_1 + S_2 + S_3}$$

$$S_1 = \frac{1}{2} \,.\, \frac{\mathrm{VRmf}}{2}.\, 1$$

$$S_2 = \frac{1}{2} \,.\, hb \,.\, (ab + 1)$$

$$S_3 = \frac{1}{2} \,.\, at \,.\, \left(\frac{\mathrm{VRmf}}{2} - hb\right).$$

Configuration A-3

$$\mathrm{s\,log_{III}} = \frac{S_1 \,.\, q_1 + S_2 \,.\, q_1 + S_3 \,.\, q_2 + S_4 \,.\, q_3}{S_1 + S_2 + S_3 + S_4}$$

$$S_1 = \frac{1}{2} \,.\, \frac{\mathrm{VRmf}}{2} \,.\, 1$$

$$S_2 = \frac{1}{2} \,.\, hb \,.\, (ab + 1)$$

$$S_3 = \frac{ha - hb}{2} \,.\, (at + ab)$$

$$S_4 = \frac{1}{2} \,.\, \left(\frac{\mathrm{VRmf}}{2} - ht\right) \,.\, at.$$

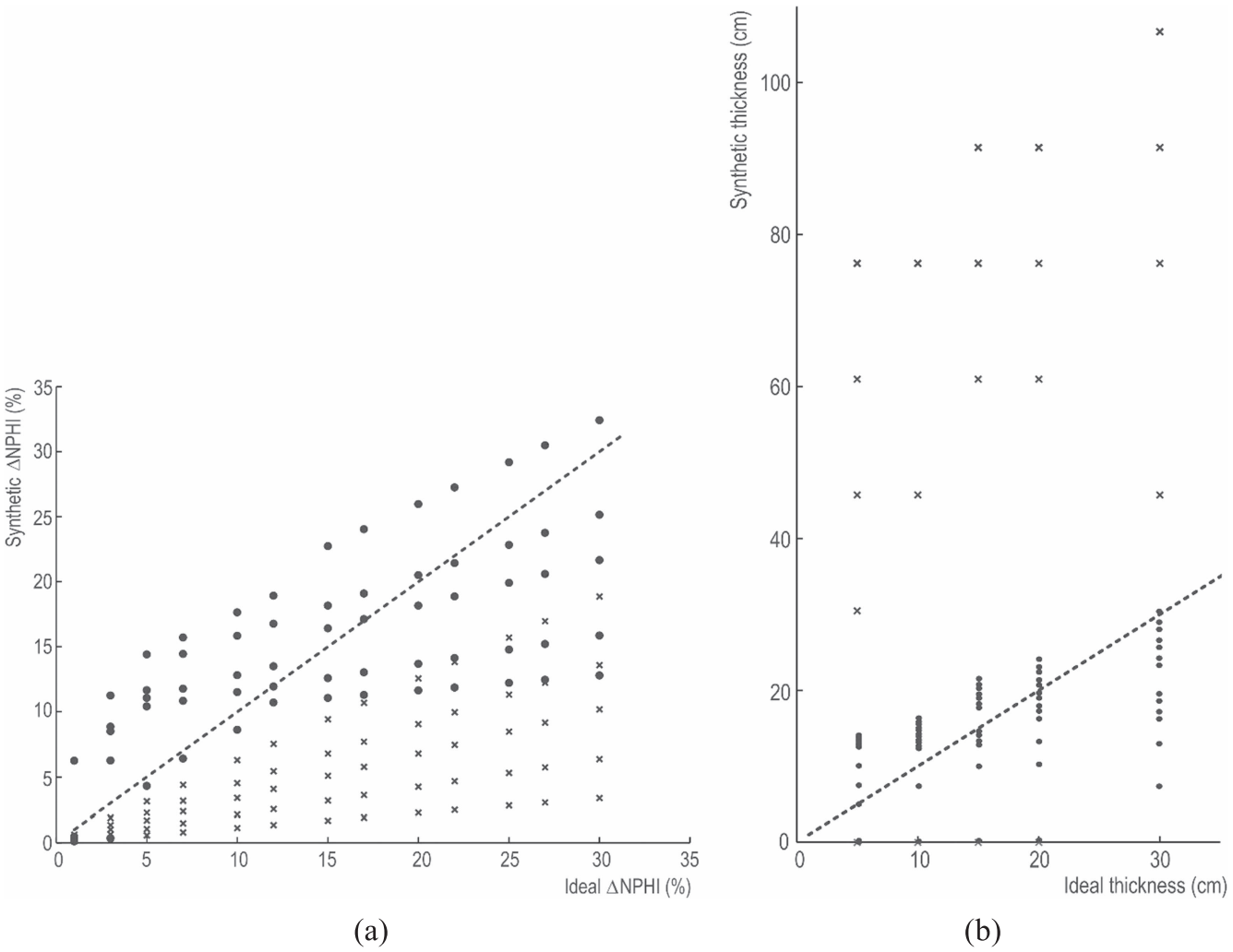

Figure 10. Deconvolution results for synthetic data. (a) Relative petrophysical values ΔNPHI (%) and (b) thickness of the thin-beds before (cross) and after (dot) reduction of the shoulder-bed effect. Each dot corresponds to a cross. Note the overlap of several crosses (b) due to limited thickness values of 5, 10, 15, 20 or 30 cm in generating ideal-logs.

Table 6. Comparison of the MSE for thin-bed characterizations. The interpretations are based on synthetic-logs versus deconvolution models (figure 10).

	MSE of synthetic-logs			MSE of deconvolution models		
	GR	RHOB	NPHI	GR	RHOB	NPHI
Petrophysical value	42.25	0.003	139.61	20.20	0.001	39.99
Thickness	2249.41	3202.01	4134.78	50.75	67.31	53.29

Configuration A-4

$$\mathrm{s\,log_{IV}} = \frac{S_1 \,.\, q_1 + S_2 \,.\, q_2 + S_3 \,.\, q_2 + S_4 \,.\, q_3}{S_1 + S_2 + S_3 + S_4}$$

$$S_1 = \frac{1}{2} \,.\, ab. \left(\frac{\mathrm{VRmf}}{2} + hb^{-}\right)$$

$$S_2 = \frac{1}{2} \,.\, (-hb^{-}) \,.\, (ab + 1)$$

$$S_3 = \frac{1}{2} \,.\, ht \,.\, (at + 1)$$

$$S_4 = \frac{1}{2} \,.\, \left(\frac{\mathrm{VRmf}}{2} - ht\right) \,.\, at.$$

Configuration A-5

$$\mathrm{s\,log_{V}} = \frac{S_1 \,.\, q_1 + S_2 \,.\, q_2 + S_3 \,.\, q_3 + S_4 \,.\, q_3}{S_1 + S_2 + S_3 + S_4}$$

$$S_1 = \frac{1}{2} \,.\, ab \,.\, \left(\frac{\mathrm{VRmf}}{2} + hb^{-}\right)$$

$$S_2 = \frac{1}{2} \,.\, (ht^{-} - hb^{-}) \,.\, (ab + at)$$

$$S_3 = \frac{1}{2} \,.\, (-ht^{-}) \,.\, (at + 1)$$

$$S_4 = \frac{1}{2} \,.\, 1 \,.\, \frac{\mathrm{VRmf}}{2}.$$

Table 7. Thin-bed characterization for ten real cases through well#1. The apparent thickness values of the thin-beds are scaled to be closer to real thickness values through deconvolution models. NAN: thin-bed curve not observed.

Case	$\sqrt{\text{MSE}}$	1	2	3	4	5	6	7	8	9	10
Depth (m)		2727.96	2803.40	2831.13	2850.49	3150.87	3156.00	3158.19	3165.20	3184.55	3186.38
ΔGR log (API)	6.50	22.10	10.17	25.72	12.79	10.40	30.67	23.00	41.32	7.41	8.80
ΔGR model (API)	4.49	32.06	17.67	32.75	19.36	14.85	34.82	27.90	47.89	12.77	14.21
GR log thickness (cm)	47.43	137.16	106.68	91.44	91.44	60.96	45.72	60.96	76.20	76.20	76.20
GR model thickness (cm)	7.12	36.46	29.52	22.48	24.63	16.11	8.28	14.01	15.42	21.06	20.83
ΔRHOB log (g cm^{-3})	0.06	0.07	0.09	0.07	0.03	NAN	0.07	0.04	0.15	NAN	0.06
ΔRHOB model (g cm^{-3})	0.03	0.10	0.17	0.13	0.08	NAN	0.13	0.09	0.18	NAN	0.14
RHOB log thickness (cm)	56.59	45.72	121.92	91.44	76.20	NAN	91.44	76.20	60.96	NAN	121.92
RHOB model thickness (cm)	8.20	16.60	33.08	25.10	17.64	NAN	25.10	18.80	28.68	NAN	29.42
ΔNPHI log (%)	11.82	9.00	14.00	4.00	5.00	9.00	14.00	4.00	11.00	4.00	1.00
ΔNPHI model (%)	6.32	24.16	29.29	15.30	14.46	20.43	29.29	11.57	22.48	17.16	12.22
NPHI log thickness (cm)	64.30	121.92	121.92	91.44	76.20	91.44	121.92	60.96	91.44	106.68	91.44
NPHI model thickness (cm)	7.30	24.95	28.66	16.67	15.13	20.38	28.66	12.10	21.87	18.96	14.45
Final thickness (cm)	7.57	26.05	30.42	21.42	19.16	18.23	20.62	14.97	21.96	20.02	21.57
Standard deviation of thickness (cm)		8.14	1.91	3.52	4.02	2.14	8.89	2.81	5.41	1.05	6.13

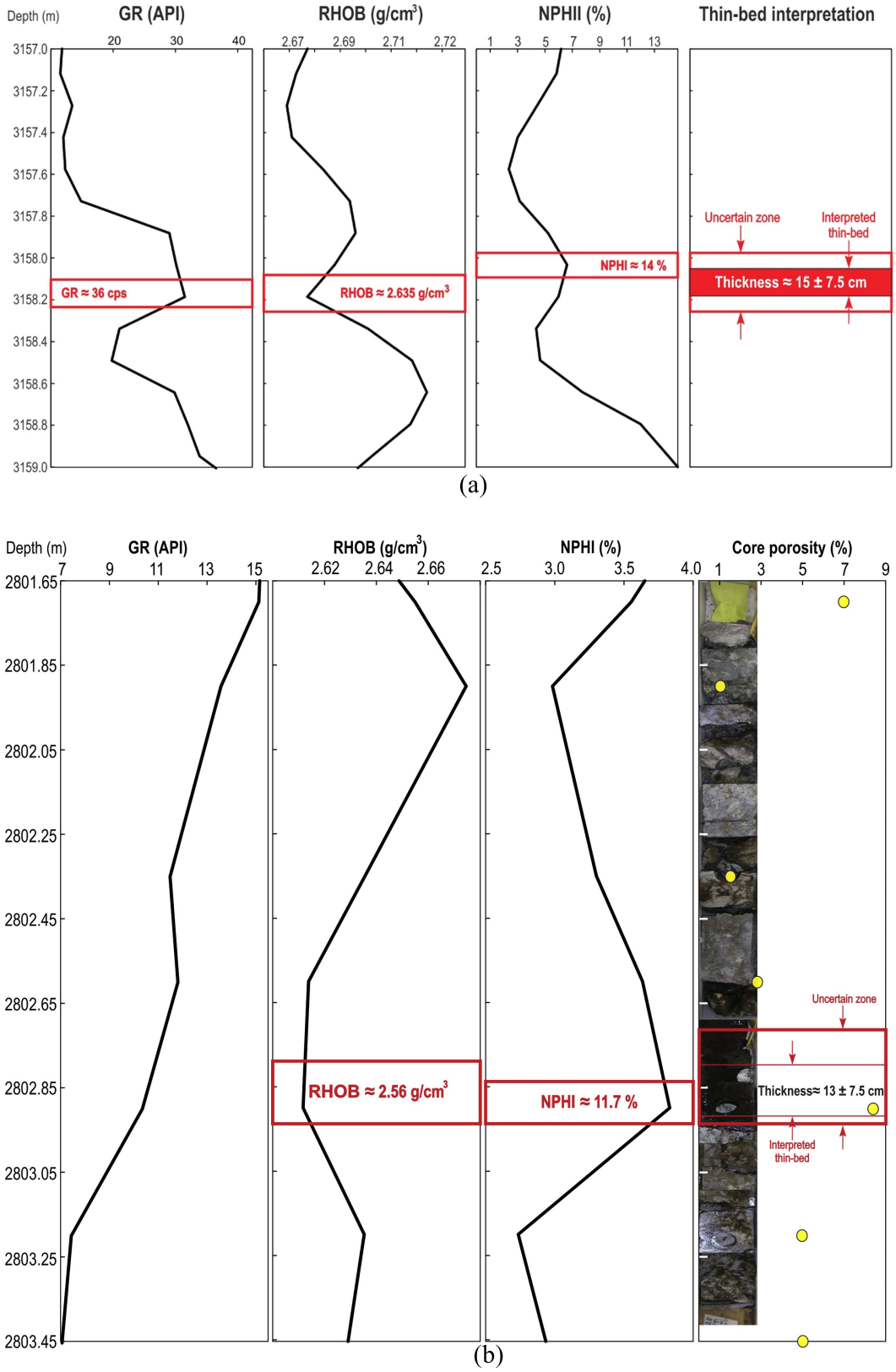

Figure 11. Two examples of thin-bed interpretation for real data. The thin-bed is first interpreted by the well-logs individually. The well-log values are amplified and given for the thin-bed. The final thickness interpretation and its associated uncertainty is provided in the rightmost track. (a) Observation#7, well#1 (table 7). (b) A case-study in well#3, verified with the core box. The yellow circles relate to core porosity (%). Thin-bed interpretation is inclined upward since the well-logs have an upward skewness.

Configuration A-6

$$s\log_{VI} = \frac{S_1 \,.\, q_2 + S_2 \,.\, q_3 + S_3 \,.\, q_3}{S_1 + S_2 + S_3}$$

$$S_1 = \frac{1}{2} \,.\, at \,.\, \left(\frac{VRmf}{2} + ht^{-}\right)$$

$$S_2 = \frac{1}{2} \,.\, (-ht^{-}) \,.\, (1 + at)$$

$$S_3 = \frac{1}{2} \,.\, 1 \,.\, \frac{VRmf}{2}.$$

Configuration A-7

$$s\log_{VII} = q_3.$$

Appendix B. Convolution form of relation (2)

In order to reach the convolution form of relation (2), the domain of functions $MF(x)$ and $q(x)$ must be extended from $-\infty$ to $+\infty$ (relations (B1) and (B2)). Considering relation (B3) the final convolution form could be achieved (relation (B4))

$$MF_e(x) = \begin{cases} MF(x);\ 0 \leqslant x \leqslant VRmf \\ 0;\ x < 0 \text{ or } VRmf < x \end{cases}, \tag{B1}$$

$$q_e(x) = \begin{cases} q(x);\ 0 \leqslant x \leqslant \mathrm{Max}\{z\} \\ 0;\ x < 0 \text{ or } \mathrm{Max}\{z\} < x \end{cases}, \tag{B2}$$

$$g(z - x) = MF_e(x), \tag{B3}$$

$$\begin{aligned} s\log(z) &= \int_{\frac{z-VRmf}{2}}^{\frac{z+VRmf}{2}} q(x) \,.\, MF(x) \,.\, dx \\ &= \int_{-\infty}^{+\infty} q_e(x) \,.\, MF_e(x) \,.\, dx \\ &= \int_{-\infty}^{+\infty} q_e(x) \,.\, g(z - x) \,.\, dx. \end{aligned} \tag{B4}$$

References

Bilardo U, Alimonti C, Chiarabelli A and Colacicchi Caetani F 1996 Formation water saturation from drilling fluid filtrate invasion: comparison of displacement modelling and induction well log response *J. Pet. Sci. Eng.* **15** 251–9

Davis A C and Christensen N B 2013 Derivative analysis for layer selection of geophysical borehole logs *Comput. Geosci.* **60** 34–40

Dempster A P 1967 Upper and lower probabilities induced by a multivalued mapping *Ann. Math. Stat.* **38** 325–39

Dempster A P 1968 A generalization of Bayesian inference *J. R. Stat. Soc.* B **30** 205–47

Desvignes G, Barthes V and Tabbagh A 1992 Direct determination of the natural remanent magnetization effect in a hole drilled in layered ground from magnetic field and susceptibility logs *Geophysics* **57** 872–84

Dewan J 1983 *Essentials of Modern Open-Hole Log Interpretation* (Tulsa, OK: PennWell Books)

Dubost F X, Zheng S Y and Corbett P W M 2004 Analysis and numerical modelling of wireline pressure tests in thin-bedded turbidites *J. Pet. Sci. Eng.* **45** 247–61

Dunham R J 1962 Classification of carbonate rocks according to depositional texture *Classification of Carbonate Rocks—A Symposium* (*AAPG Memoir* vol 1) (Tulsa, OK: AAPG) 108–21

Ellis D V and Singer J M 2007 *Well Logging for Earth Scientists* 2nd edn (Dordrecht: Springer) (https://doi.org/10.1007/978-1-4020-4602-5)

Gallet Y and Courtillot V 1989 Modeling magnetostratigraphy in a borehole *Geophysics* **54** 973–83

Ghabeishavi A, Vaziri-Moghaddam H, Taheri A and Taati F 2010 Microfacies and depositional environment of the Cenomanian of the Bangestan anticline, SW Iran *J. Asian Earth Sci.* **37** 275–85

Ghazban F 2009 *Petroleum Geology of the Persian Gulf* (Tehran: University of Tehran)

Gringarten E and Deutsch C V 2001 Teacher's aide variogram interpretation and modeling *Math. Geol.* **33** 507–34

Heidari Z, Torres-Verdín C and Preeg W E 2012 Improved estimation of mineral and fluid volumetric concentrations from well logs in thinly bedded and invaded formations *Geophysics* **77** WA79–98

Heidari Z and Torres-Verdín C 2014 Inversion-based detection of bed boundaries for petrophysical evaluation with well logs; applications to carbonate and organic-shale formations *Interpretation* **2** T129–42

Ijasan O, Torres-Verdín C and Preeg W E 2013 Inversion-based petrophysical interpretation of logging-while-drilling nuclear and resistivity measurements *Geophysics* **78** D473–89

Ijasan O, Torres-Verdín C, Preeg W E, Rasmus J and Stockhausen E 2014 Field examples of the joint petrophysical inversion of resistivity and nuclear measurements acquired in high-angle and horizontal wells *Geophysics* **79** D145–59

James G A and Wynd J G 1965 Stratigraphic nomenclature of Iranian oil consortium agreement area *AAPG Bull.* **49** 2182–245

Kinsland G L, Borst C, Das K and McWhorter M 2010 Interpretation, visualization and presentation of digital well-log data in 3D virtual reality space; application to mapping of coals *Am. Assoc. Pet. Geologists* 2010

Majid A A and Worthington P F 2012 Definitive petrophysical evaluation of thin hydrocarbon reservoir sequences *SPE Reservoir Eval. Eng.* **15** 584–95

Mehrabi H, Rahimpour-Bonab H, Hajikazemi E and Jamalian A 2015 Controls on depositional facies in upper cretaceous carbonate reservoirs in the Zagros area and the Persian Gulf, Iran *Facies* **61** 1–24

Mukaka M M 2012 A guide to appropriate use of Correlation coefficient in medical research *Malawi Med. J.* **24** 69–71

Nyquist H 1924 Certain factors affecting telegraph speed *Bell Syst. Tech. J.* **3** 324–46

Ortega E, Torres-Verdín C and Preeg W E 2015 2D inversion-based interpretation of logging-while-drilling thermal-neutron and gamma-ray time decays *Geophysics* **80** D247–63

Peyret A, Torres-Verdín C and Xu Y 2006 Assessment of shoulder-bed, invasion, and lamination effects on borehole sonic logs; a numerical sensitivity study *SPWLA 47th Annual Logging Symposium (Veracruz, Mexico)* p 156

Qi L and Carr T R 2006 Neural network prediction of carbonate lithofacies from well logs, Big Bow and Sand Arroyo Creek fields, southwest Kansas *Comput. Geosci.* **32** 947–64

Razin P, Taati F and van Buchem F S P 2010 Sequence stratigraphy of Cenomanian–Turonian carbonate platform margins (Sarvak Formation) in the High Zagros, SW Iran: an outcrop reference model for the Arabian Plate *Geol. Soc.* **329** 187–218

Read J F 1985 Carbonate platform facies models *AAPG Bull.* **69** 1–21

RP 2007 *Oil and Gas Glossary* (Perth: Recruitment Specialists in Upstream Oil and Gas) (http://resourcepersonnel.com/) (accessed 2016.02.01)

Sanchez Ramirez J A, Torres-Verdín C, Wolf D, Wang G L, Mendoza A, Liu Z and Schell G 2010 Field examples of the combined petrophysical inversion of gamma-ray, density, and resistivity logs acquired in thinly bedded clastic rock formations *Petrophysics* **51** 247–63

Schlumberger 2015 *Wireline Services Catalog (Schlumberger Methods)* (Tehran: Well Services of Iran)

Sengupta M K 1987 Time-offset-frequency-amplitude panels for seismic identification of hydrocarbons *United States Patent* US4694438 A

Sengupta M K, Lange J N and Almoghrabi H A 1989 Lithology discrimination for thin layers using wavelet signal parameters; discussion and reply *Geophysics* **54** 789–789

Tarantola A 2005 *Inverse Problem Theory and Methods for Model Parameter Estimation* (Philadelphia, PA: Society for Industrial and Applied Mathematics) (https://doi.org/10.1137/1.9780898717921.bm)

Torres-Verdín C, Sanchez Ramirez J, Mendoza A, Wang G L and Wolf D 2010 Field examples of the joint petrophysical inversion of gamma-ray, density and resistivity logs acquired in thinly-bedded clastic rock formations *Petrophysics* **51** 165–6

Vincent B, van Buchem F S P, Bulot L G, Jalali M, Swennen R, Hosseini A S and Baghbani D 2015 Depositional sequences, diagenesis and structural control of the Albian to Turonian carbonate platform systems in coastal Fars (SW Iran) *Mar. Pet. Geol.* **63** 46–67

Zarasvandi A, Charchi A, Carranza E J M and Alizadeh B 2008 Karst bauxite deposits in the Zagros Mountain Belt *Iran Ore Geology* **34** 521–32